



Influence of acoustofluidic parameters on velocity streaming of sonicated medical microbubbles

Hussain Alsadiq (1), Karnaker Reddy (2), Harendra Parekh (2) and Martin Veidt (1).

(1) Mechanical and Mining School, University of Queensland, Brisbane, Australia.

(2) School of Pharmacy, University of Queensland, Brisbane, Australia.

ABSTRACT

Ultrasonic theranostics using echogenic bubbles allow real-time traceability and site-specific, on demand medicine delivery. Ultrasonic manipulation of microbubbles is studied through illustrating the effect of acoustofluidic properties on flow and interaction of bubble populations. Significant displacement and clustering of medical microbubbles are observed for excitations resulting in acoustic pressures as low as 6 kPa. Microbubble displacements are found to be negligible at 4 kPa. The measured velocities show good agreement with analytical calculations at pressure levels below the threshold of non-linear bubble behaviour. Higher pressures caused faster bubble movement and higher frequencies resulted in faster cluster formation. An extreme effect is also reported where the secondary radiation force overcomes the primary radiation force, which results in bubbles moving towards the acoustic source.

1 INTRODUCTION

The use of microbubbles as ultrasonic contrast agents (UCA), has been proven efficient in enhancing diagnostic imaging (Cosgrove 2006), and have a potential theranostic use due to their biocompatibility and real time traceability. They are approved for in-vivo use by the American Food and Drug Administration, and there have been intensive studies on their production and chemical composition (Quaia 2007), shell and acoustic properties (Hoff 2001) and drug delivery ability (Fan et al. 2013). However, the streaming flow experienced by a population of acoustically activated microbubbles is not yet fully understood.

Efficient transportation of microbubbles is dependent on bubble size, stability, mechanical properties of the medium and the acoustic parameters of the driving wave. Stabilising shells of lipid and other encapsulation media have been studied analytically through modifying the Rayleigh-Pleasant equation to include the effect of the shell, and have been validated experimentally by measuring the dynamic response of the bubble radius due to sonication optically (van der Meer et al. 2007) or using laser scattering (Guan and Matula 2004). Shell properties have also been studied through measuring acoustic scattering and attenuation caused by bubble populations to investigate shell mechanical properties (Paul et al. 2014, Hoff 2001). The shell friction is directly proportional to the damping coefficient, which has an influence on slowing the bubble velocity. The mechanical properties of the fluid surrounding the bubbles affect the oscillation and translation of the bubbles. For example, bubbles suspended in higher viscosity fluids experience slower motion if all other parameters are constant. Finally, the transmitted pressure and the ratio of resonance to excitation frequency are non-linearly related to the bubbles' speed, (Kotopoulos and Postema 2010, Dayton et al. 1997).

The streaming flow of microbubble populations have been investigated using Particle Image Velocimetry (PIV) of fluorescent tracers added to a solution of sonicated SonoVue™ bubbles (Cho, Chung, and Rhee 2015). The study found that the velocity of the bubbles increases when frequency increases close to the resonance frequency, and the effect of pressure on velocity is minimal. However, cluster formation and translation are slower when the acoustic pressure is reduced. Although this study verified that the tracers do not move due to radiation force directly. Hence, it is highly possible that the tracers increased the drag force and slowed the movement of the bubbles, noting that the tracers' size is more than double the bubbles' size. Cluster formation, translation and collisions caused by sonication of Definity™ microbubble populations have been studied in detail (Kotopoulos and Postema 2010). Clusters of microbubbles were found to behave as one mega-bubble entity which simplifies ultrasonic manipulation.

Definity™ microbubbles are the smallest commercially approved ultrasonic contrast agents with a mean diameter of 1.1-3.3 μm (Tsuge 2014), although even smaller phospholipid nanobubbles have been demonstrated to be feasible and stable agents for safe and effective drug delivery (Thakur et al. 2017). Definity™ consists of

octafluoropropane (C_3F_8) gas encapsulated into a lipid shell. Its shell properties have been acoustically characterised and it was found that it has $0.15 \pm 0.02 \times 10^{-6}$ kg/s friction factor S_f and 1.64 ± 0.33 N/m shell stiffness S_p , when excited at 7-15 MHz (Faez, Goertz, and De Jong 2011), and its resonance frequency is 2.7 MHz (Kimmel et al. 2007). However, the latter varies significantly for samples with different diameters.

This paper investigates the behaviour of suspended Definity™ microbubbles due to biologically safe acoustic waves *i.e. acoustic waves with low mechanical and thermal indices*. The mechanical index of the excitation waves in this study range between $MI=0.0023-0.004$, which has been shown to have no detectable bioeffect (*Guidelines for the safe use of diagnostic ultrasound equipment*, 2010). The thermal index is dependent on the biological medium. However with the excitation powers used in this study, a noticeable thermal change in a medium with acoustic characteristics similar to human tissue requires several hours of exposure (Bigelow et al. 2011). The acoustic pressures used in this study ensure a linear bubble behaviour as the nonlinear behaviour of Definity™ microbubbles observed at minimum acoustic pressure of 13 kPa (Helfield and Goertz 2013). This linear behaviour is expected to simplify the controlled manipulation of the microbubbles.

2 METHODOLOGY

A 1.75mm diameter microfluidic channel of Polydimethylsiloxane (PDMS) was manufactured using a ratio of 5:1 elastomer to curing agent (Sylgard® 148) with an average wall thickness of 0.25 mm (Figure 1). The channel was then mounted in a 135 mm × 195 mm × 51 mm water bath filled with demineralised water, at a distance of 31 mm from an immersion transducer (V381 Olympus®) as illustrated in (Figure 2).



Figure 1: A cross sectional view of the PDMS microfluidic channel.

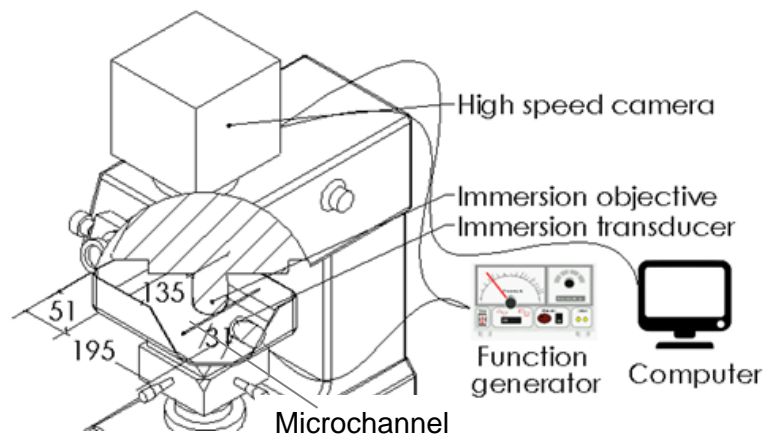


Figure 2 : Schematic of the experimental setup.

The microfluidic channel was positioned under the $\times 40$ magnification immersion objective of a Leica® DM 1750 M optical microscope with a Photron®, UX100 high speed camera. The camera was connected to a computer for data acquisition and image processing, and to the sync output of the arbitrary function generator (Rigol®, DG4062) to trigger recording. The function generator was used to excite the transducer using the excitation parameters outlined in section 2.2.

2.1 Microbubble Preparation

A Definity™ vial (1.5mL, Bristol-Mayers®) was agitated using a VialMix™ for 45 s to activate the bubbles according to the manufacturer's instructions, and then diluted in 15 mL of demineralised water. The size distribution of the bubbles was measured using dynamic light scattering (Malvern®, Zetasizer™ Nano ZS). It was found that the population had an average diameter of 835.9 nm with standard deviation of 130.9 nm. This size differs from the size claimed by the manufacturer of 1.1-3.3 μm . This difference could be due to storage effects and temperature changes. The vials before and after activation were stored at 3.7 °C, and the experiments were performed at 25.1 °C.

2.2 Measuring Acoustic Pressure Inside the Channel

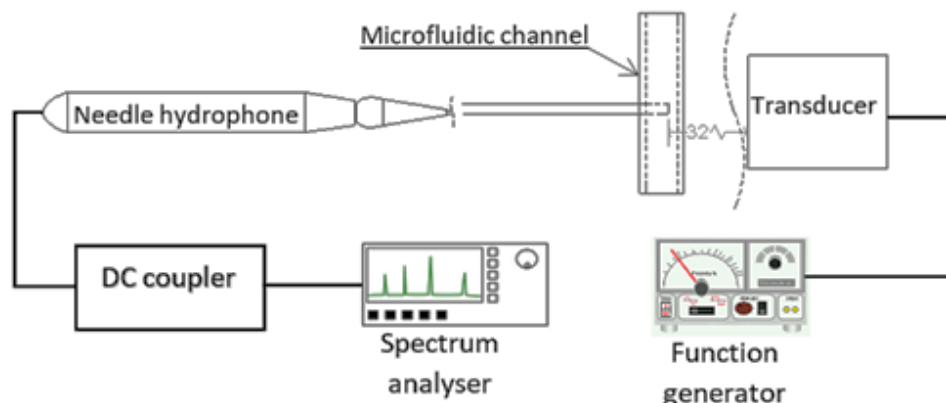


Figure 3: Experimental setup for measuring the acoustic pressure inside the microfluidic channel (not to scale).

A preliminary experiment was conducted to measure the acoustic pressure inside the channel. The transducer was positioned 32 mm from the 0.2 mm diameter active element of a needle hydrophone (Precision®), which was placed inside the channel as illustrated in (Figure 3). The hydrophone readings were acquired using a spectrum analyser (Rigol® DSA815TG) and converted into kPa using the hydrophone manufacturer’s calibration report. The excitation voltages were adjusted to produce 4, 6 and 8 kPa at 3, 3.5 and 4 MHz as described in Table 1. The received voltages reported in the table are averages of 100 readings. The readings were averaged due to noise floor fluctuations of $\pm 5 \mu\text{V}$.

Table 1 : Acoustic pressure developed inside the channel due to corresponding excitation voltages.

Frequency (MHz)	Excitation (V)	Response (μV)	Hydrophone sensitivity (mV/MPa)	Pressure in channel (kPa)
3	10	279 ± 5	69	4 ± 0.3
3	15	410 ± 5	69	5.9 ± 0.3
3	20	548 ± 5	69	7.9 ± 0.3
3.5	4	274 ± 5	67.5(interpolated)	4.1 ± 0.3
3.5	13.6	411 ± 5	67.5(interpolated)	6.1 ± 0.3
3.5	19.4	547 ± 5	67.5(interpolated)	8.1 ± 0.3
4	10	280 ± 5	66	4.2 ± 0.3
4	14.6	412 ± 5	66	6.2 ± 0.3
4	19.6	551 ± 5	66	8.3 ± 0.3

2.3 Data Analysis

The displacement of the microbubbles due to sonication is captured at 250 fps for approximately 35 s in each experiment and analysed using FASTCAM™ (Photron®). Five single bubbles for each experiment were selected randomly and traced, and their displacements were acquired. In addition, the instantaneous velocity of the flow was calculated through particle image velocimetry using PIVLab™ (Thielicke and Stamhuis 2014b, Thielicke and Stamhuis 2014a) and post-processed using tools introduced in (Garcia 2011).

3 RESULTS AND DISCUSSION

The experimental results showed no significant displacement in the direction of the excitation at 4 kPa acoustic pressure at 3, 3.5 and 4 MHz. However, significant displacement of bubbles were observed when excited at 6 kPa and 8 kPa at the three frequencies. In this section, the optical observations are discussed, and the velocities of single bubbles are deduced and compared to analytical calculations. Finally, the effect of secondary Bjerknes forces when acting against the primary radiation forces is discussed.

3.1 Optical Observation

The time sequence of a representative experiment is shown in Figure 4. Since the field of view of the objective is smaller than the diameter of the channel, some of the bubbles and bubble clusters will move outside of the objective view field during the observation period, as seen in the clusters located at the bottom of the frames between 2.6 s-3.6 s.

The bubbles population was excited with a 3.5 MHz, 8 kPa acoustic wave. At the beginning of the excitation, bubbles close to each other are attracted to one another to form clusters as seen in the first two rows, while slowly moving away from the acoustic source to the right. The attraction force caused by the secondary Bjerknes force of larger clusters on smaller clusters is higher than the other way around. Thus, for example, the small cluster indicated by the red arrow in the 1.4 s frame is moving towards the larger cluster located above it and is absorbed into it. This phenomenon is consistently observed in the other experiments where the small clusters move towards the larger, denser clusters. This is because of the drag force dependency on the cluster radius, where larger bubble clusters have a larger drag force than small clusters (Kotopoulos and Postema 2010). And since the attraction force between them is equal, the smaller cluster moves toward the larger one.

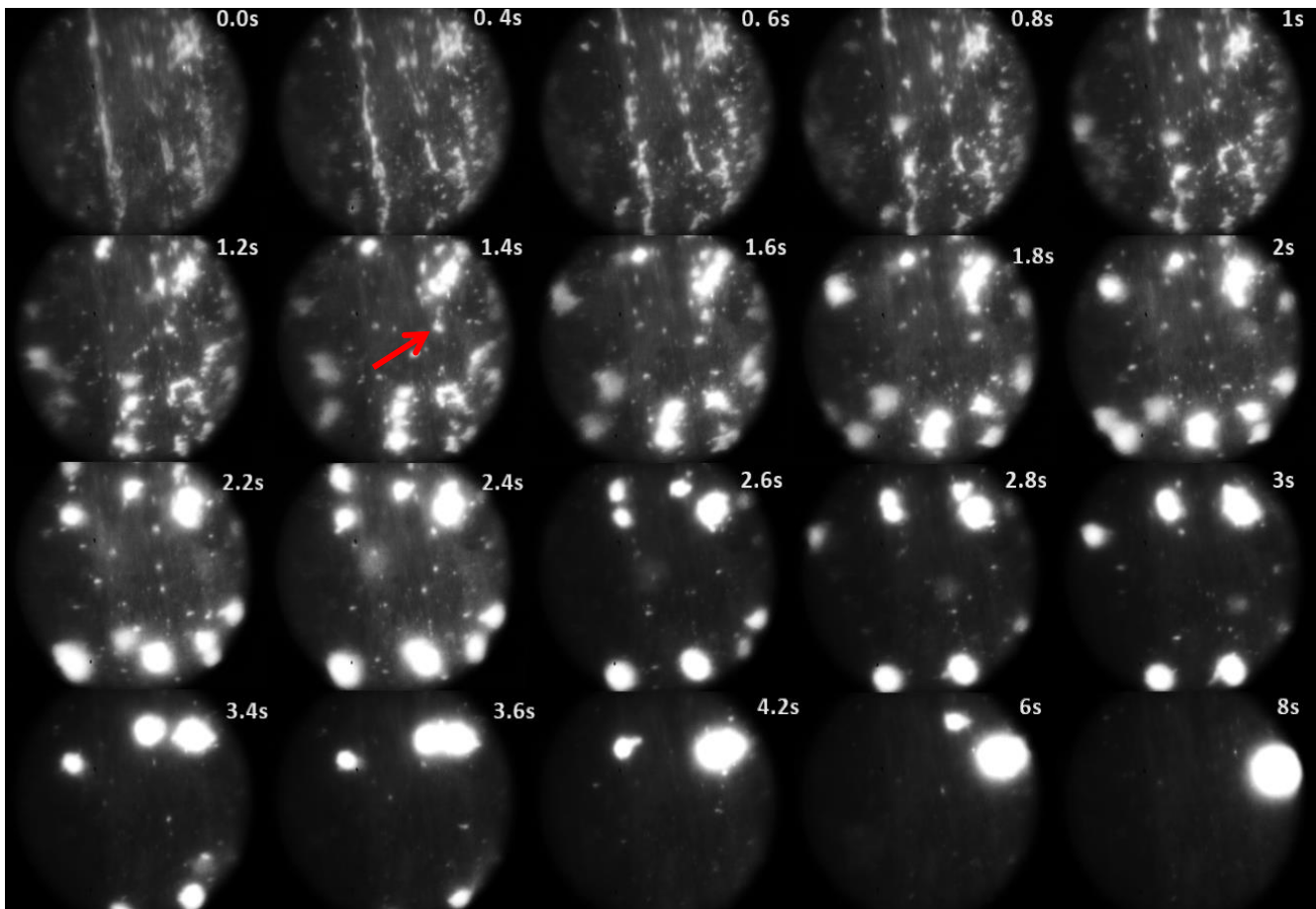


Figure 4: Microbubble displacement due to a 3.5 MHz, 8 kPa acoustic wave. The field of view diameter is 530 μ m per frame. Red arrow indicates a small cluster before being attracted to a larger cluster.

The bubble clusters start to accelerate in the direction of the acoustic wave after the first second where bubbles movement is dominated by cluster formation rather than movement away from the acoustic source on the left. The velocity of single traced microbubbles were measured over one second for five selected bubbles to be $10.15 \pm 0.66 \mu\text{m/s}$, and the velocity fields of the bubbles showed a maximum displacement rate of 35 $\mu\text{m/s}$. This will be discussed in detail in sections 3.2 and 3.3.

It has to be noted that until the very end of the 35 s acoustic excitation, the bubbles within the clusters maintained their individual shells and no sign of coalescence was observed in any of the experiments. Although the acoustic excitation continued for 35 s, the last bubble cluster in Fig. 4 maintained its location after eighth seconds for the 3.5 MHz, 8 kPa acoustic excitation. Thus, no further frames are shown.

Faster cluster formation rates were observed for higher frequencies at the same pressure levels. However, the more notable observation was the increase in the velocities of individual bubbles at 8 kPa compared to 6 kPa excitation pressure at the same frequencies, which is discussed in the next section.

3.2 Streaming Velocity Field

As single bubbles tend to cluster fast, bubble and cluster flows have a large variation in velocity. The streaming velocity fields have thus been mapped using PIV as described in section 2.3. Figure 5 shows the velocity fields of bubble populations after 0.4 s of excitation for 6 kPa and 8 kPa excitation pressure at 3.5 MHz, respectively. The maximum velocities of bubble clusters were 25 $\mu\text{m/s}$ and 35 $\mu\text{m/s}$ for 6 kPa and 8 kPa excitation pressures respectively. In the case of the 6 kPa pressure level, higher velocities occur more frequently closer to the excitation source on the left. High velocity areas are more homogeneously distributed for 8 kPa excitation pressure.

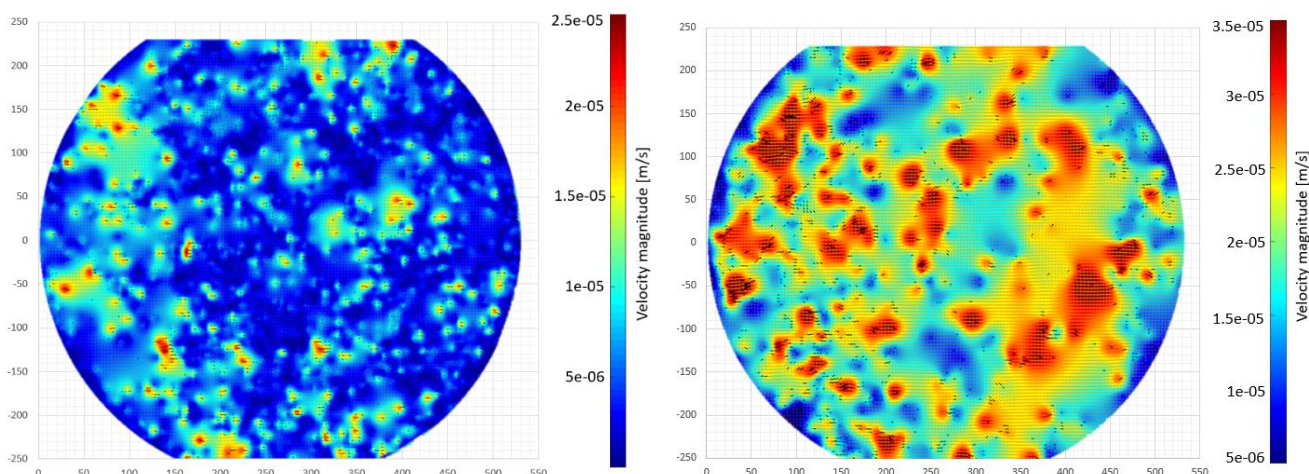


Figure 5: Streaming velocity fields of bubble populations sonicated by 6 kPa, 3.5 MHz (left) and 8 kPa, 3.5 MHz (right) acoustic waves.

Lower pressures are preferred for *in vivo* use in the medical practice, due to their lower bioeffect. The experiments attempted in this study have shown that an acoustic wave of 6 kPa at 4 MHz is sufficient excitation for moving bubbles a distance more than 0.5 mm over 19 s.

3.3 Single Bubble Velocity

Assuming that the first radiation force and the drag force are dominating the system flow, and other factors such as Bjerknes force have an insignificant effect, Kotopoulis and Postema applied an integral form of Newton's second law to derive the following equation for the velocity of a single bubble in an acoustic field (Kotopoulis and Postema 2010):

$$v = \frac{4P_a^2}{\rho c f \eta C_d Re} \frac{\delta \left(\frac{f_0}{f}\right)}{\left[\left(\frac{f_0}{f}\right)^2 - 1\right]^2 + \left[\delta \left(\frac{f_0}{f}\right)\right]^2} \left[1 - e^{-\left(\frac{3\eta C_d Re}{8\rho R_0^2} t\right)}\right] \quad (1)$$

where P_a is the acoustic pressure, ρ is the density of the surrounding fluid, c is the speed of sound in the fluid, C_d is the drag coefficient, Re is the Reynold's number, δ is the damping coefficient of the fluid, f_0 is the resonance frequency of the bubble, f is the excitation frequency, R_0 is the bubble radius, and η is the dynamic shear viscosity of the fluid.

Assuming negligible thermal losses, the total damping coefficient δ can be considered as the summation of the damping due to radiation δ_{rad} , viscosity δ_{vis} , and shell friction δ_{sh} (de Jong et al. 1992) such as:

$$\delta_{rad} = \frac{\omega R}{c} \quad (2)$$

$$\delta_{vis} = \frac{4\eta}{\omega \rho R^2} \quad (3)$$

$$\delta_{sh} = \frac{S_f}{4\pi\omega\rho R^3} \quad (4)$$

where ω is the angular frequency ($2\pi f$). The resonance frequency is calculated as (Goertz, de Jong, and van der Steen 2007):

$$f_0 = \frac{1}{2\pi} \sqrt{\frac{3\gamma P_0}{\rho R^2} + \frac{2S_p}{\rho R^3}} \quad (5)$$

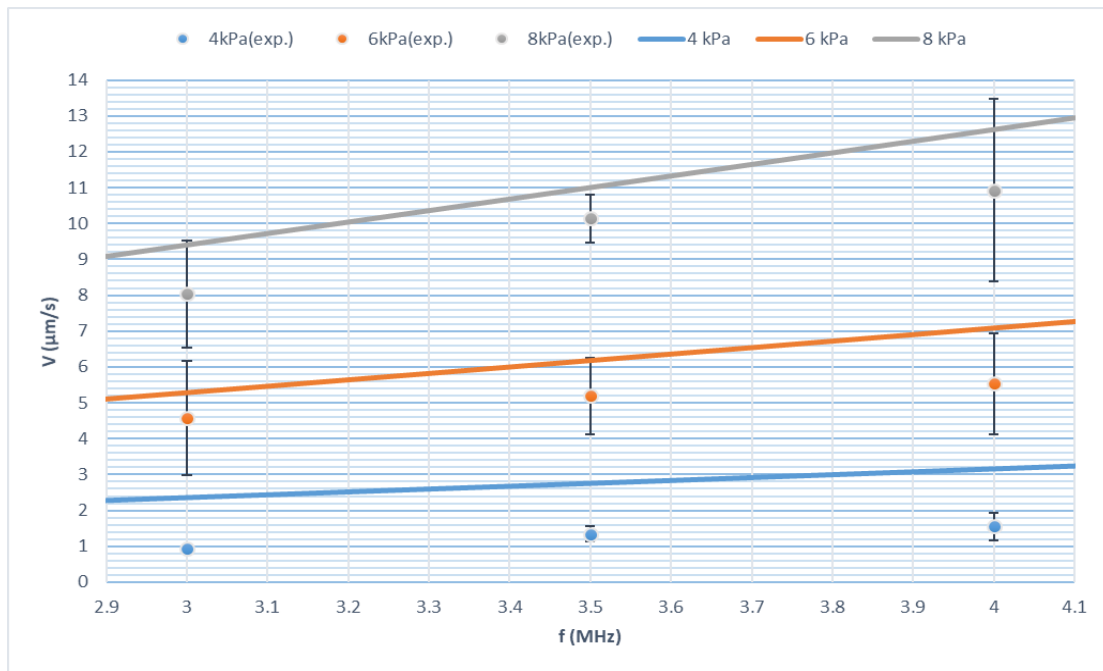


Figure 6: Experimental and analytical velocities of a single microbubble as a function of frequency at three different pressures.

Substituting equations 2, 3, 4 and 5 into 1 gives the velocity of a single bubble at a specific radius, pressure and frequency. Figure 6 shows in bold lines the velocity as a function of frequency for the three pressure levels. The results of the experimental measurements are shown as individual points. Each point represents the average velocity over one second of five single bubbles. The experimental results are consistently lower than the analytical results. In the case of the 6 kPa and 8 kPa excitation which show some distinct bubble motion, the experimental velocities are between 10% and 22% lower than the theoretical predictions. This could be because of the shell friction $0.15 \pm 0.02 \times 10^{-6}$ kg/s used to calculate the shell damping. As mentioned previously, this figure was measured at 7-15 MHz for larger diameter Definity™ bubbles (Faez, Goertz, and De Jong 2011). Using a shell friction parameter of 0.1×10^{-6} kg/s results in a perfect fit of the experimental data. However acoustic characterisation of the shell parameters at the frequency used were not attempted in this study nor found in previous studies.

3.4 Secondary Radiation Force Effect

Microbubble and microbubble cluster movement in the opposite direction of the propagating wave are frequently observed. Figure 7 shows an example of the movement of a smaller cluster towards a bigger cluster. These observations imply that the secondary radiation force is overcoming the primary radiation force, which results in bubbles or clusters moving towards the excitation source. This is an interesting phenomenon that needs further investigation, since it may have critical implications on the design and application of ultrasonic microbubble manipulation systems for safe and efficient drug delivery.

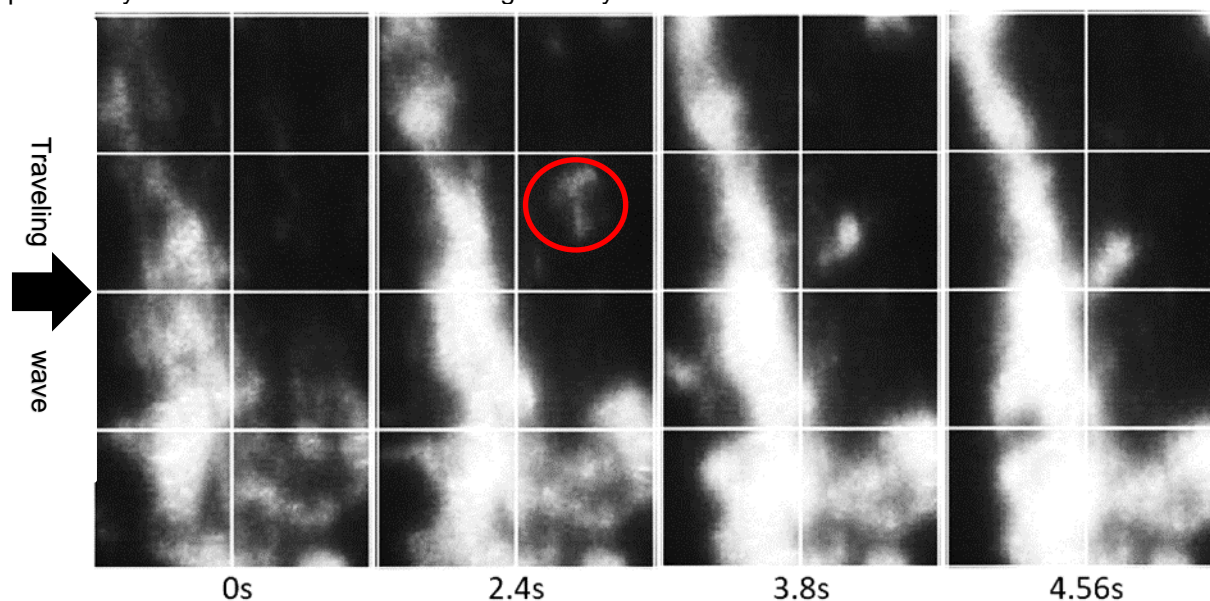


Figure 7: Small cluster of bubbles moving opposite to the wave (8kPa,4MHz) propagation direction. Each division has 50 μ m side length.

CONCLUSIONS

The influence of acoustofluidic properties on movement and interaction of medical diagnostic microbubbles populations have been studied. The results have shown that:

- Significant displacement and clustering of microbubbles was observed when excited at acoustic pressures of 6 kPa and 8 kPa at excitation frequencies between 3 MHz and 4 MHz. However, bubbles barely moved at an excitation pressure of 4 kPa at the aforementioned frequencies.
- The results showed that significant bubble movement is created at biologically safe acoustic pressure levels well below the threshold pressure of non-linear bubble behaviour.
- The measured velocities of individual bubbles were in good agreement with theoretical predictions based on a model which assumes that first radiation and drag forces dominate the bubble-fluid interaction. Higher pressures and higher frequencies result in faster bubble movements. The comparison also showed that accurate measurement of the damping coefficient of the microbubble shell at the specific acoustofluidic parameters and bubble diameters is necessary to accurately predict bubble velocity.
- Significant clustering started within the first couple of seconds for all excitation parameters that showed clear bubble movement. Higher frequencies resulted in a faster clustering rate.

Future work will focus on developing analytical and numerical models to predict the acoustofluidic behaviour of medical micro bubbles at pressures and frequencies that have been demonstrated to be biologically safe. This will allow designing accurate drug delivery systems for specific medical applications.

ACKNOWLEDGEMENTS

The authors are grateful for the support of The Saudi Arabian Cultural Mission in the form of a scholarship for the first author.

*Senior author email: m.veidt@uq.edu.au

REFERENCES

- Bigelow, Timothy A, Charles C Church, Kurt Sandstrom, John G Abbott, Marvin C Ziskin, Peter D Edmonds, Bruce Herman, Kai E Thomenius, and Tat Jin Teo. 2011. "The thermal index: its strengths, weaknesses, and proposed improvements." *Journal of Ultrasound in Medicine* 30 (5):714-734.
- Cho, Eunjin, Sang Kug Chung, and Kyehan Rhee. 2015. "Streaming flow from ultrasound contrast agents by acoustic waves in a blood vessel model." *Ultrasonics* 62:66-74.
- Cosgrove, David. 2006. "Ultrasound contrast agents: an overview." *European journal of radiology* 60 (3):324-330.
- Dayton, Paul A, Karen E Morgan, Alexander L Klivanov, Gary Brandenburger, Kathryn R Nightingale, and Katherine W Ferrara. 1997. "A preliminary evaluation of the effects of primary and secondary radiation forces on acoustic contrast agents." *IEEE transactions on ultrasonics, ferroelectrics, and frequency control* 44 (6):1264-1277.
- de Jong, Nico, Lars Hoff, Tore Skotland, and Nicolaas Bom. 1992. "Absorption and scatter of encapsulated gas filled microspheres: theoretical considerations and some measurements." *Ultrasonics* 30 (2):95-103.
- Faez, Telli, David Goertz, and Nico De Jong. 2011. "Characterization of Definity™ ultrasound contrast agent at frequency range of 5–15 MHz." *Ultrasound in medicine and biology* 37 (2):338-342.
- Fan, Ching-Hsiang, Chien-Yu Ting, Hao-Li Liu, Chiung-Yin Huang, Han-Yi Hsieh, Tzu-Chen Yen, Kuo-Chen Wei, and Chih-Kuang Yeh. 2013. "Antiangiogenic-targeting drug-loaded microbubbles combined with focused ultrasound for glioma treatment." *Biomaterials* 34 (8):2142-2155.
- Garcia, Damien. 2011. "A fast all-in-one method for automated post-processing of PIV data." *Experiments in fluids* 50 (5):1247-1259.
- Goertz, David E, Nico de Jong, and Antonius FW van der Steen. 2007. "Attenuation and size distribution measurements of Definity™ and manipulated Definity™ populations." *Ultrasound in medicine & biology* 33 (9):1376-1388.
- Guan, Jingfeng, and Thomas J Matula. 2004. "Using light scattering to measure the response of individual ultrasound contrast microbubbles subjected to pulsed ultrasound in vitro." *The Journal of the Acoustical Society of America* 116 (5):2832-2842.
- Helfield, Brandon L, and David E Goertz. 2013. "Nonlinear resonance behavior and linear shell estimates for Definity™ and MicroMarker™ assessed with acoustic microbubble spectroscopy." *The Journal of the Acoustical Society of America* 133 (2):1158-1168.
- Hoff, Lars. 2001. *Acoustic characterization of contrast agents for medical ultrasound imaging*: Springer Science & Business Media.
- Kimmel, Eitan, Boris Krasovitski, Assaf Hoogi, Daniel Razansky, and Dan Adam. 2007. "Subharmonic response of encapsulated microbubbles: Conditions for existence and amplification." *Ultrasound in medicine & biology* 33 (11):1767-1776.
- Kotopoulos, Spiros, and Michiel Postema. 2010. "Microfoam formation in a capillary." *Ultrasonics* 50 (2):260-268.
- Paul, Shirshendu, Rahul Nahire, Sanku Mallik, and Kausik Sarkar. 2014. "Encapsulated microbubbles and echogenic liposomes for contrast ultrasound imaging and targeted drug delivery." *Computational mechanics* 53 (3):413-435.
- Quaia, Emilio. 2007. "Microbubble ultrasound contrast agents: an update." *European radiology* 17 (8):1995-2008.
- Society, Prepared by the Safety Group of the British Medical Ultrasound. 2010. "Guidelines for the safe use of diagnostic ultrasound equipment." *Ultrasound* 18 (2):52-59.
- Thakur, Sachin S, Micheal S Ward, Amirali Popat, Nicole B Flemming, Marie-Odile Parat, Nigel L Barnett, and Harendra S Parekh. 2017. "Stably engineered nanobubbles and ultrasound-An effective platform for enhanced macromolecular delivery to representative cells of the retina." *PLoS one* 12 (5):e0178305.
- Thielicke, W, and EJ Stamhuis. 2014a. "PIVlab-Time-Resolved Digital Particle Image Velocimetry Tool for MATLAB (version: 1.35)." *J. Open Res. Software* 2 (1):e30.
- Thielicke, William, and Eize Stamhuis. 2014b. "PIVlab—towards user-friendly, affordable and accurate digital particle image velocimetry in MATLAB." *Journal of Open Research Software* 2 (1).
- Tsuge, Hideki. 2014. *Micro-and Nanobubbles: Fundamentals and Applications*: CRC Press.
- van der Meer, Sander M, Benjamin Dollet, Marco M Voormolen, Chien T Chin, Ayache Bouakaz, Nico de Jong, Michel Versluis, and Detlef Lohse. 2007. "Microbubble spectroscopy of ultrasound contrast agents." *The Journal of the Acoustical Society of America* 121 (1):648-656.